Can superabsorbent polymers be used as rheology modifiers for cementitious materials in the context of 3D concrete printing?

Chen, Yu; Liang, Minfei; Zhang, Yu; Li, Zhenming; Šavija, Branko; Schlangen, Erik; Çopuroğlu, Oğuzhan

DOI
10.1016/j.conbuildmat.2023.130777

Publication date
2023

Document Version
Final published version

Published in
Construction and Building Materials

Citation (APA)
Chen, Y., Liang, M., Zhang, Y., Li, Z., Šavija, B., Schlangen, E., & Çopuroğlu, O. (2023). Can superabsorbent polymers be used as rheology modifiers for cementitious materials in the context of 3D concrete printing? *Construction and Building Materials*, *371*, Article 130777. https://doi.org/10.1016/j.conbuildmat.2023.130777

Construction and Building Materials 371 (2023) 130777

Contents lists available at ScienceDirect

Construction and Building Materials

journal homepage: www.elsevier.com/locate/conbuildmat

Can superabsorbent polymers be used as rheology modifiers for cementitious materials in the context of 3D concrete printing?

Yu Chen, Minfei Liang *, Yu Zhang, Zhenming Li, Branko Šavija, Erik Schlangen, Oğuzhan Çopuroğlu

Microlab, Faculty of Civil Engineering and Geosciences, Delft University of Technology, Delft, the Netherlands

ARTICLE INFO

Keywords:
Limestone-calcined clay-cement
Superabsorbent polymer
Structural build-up
Hydration kinetics
Rheology modifier
Autogenous shrinkage

ABSTRACT

Autogenous shrinkage may be a critical issue concerning the use of limestone-calcined clay-cement (LC3) in high-performance concrete and 3D printable cementitious materials, which have relatively low water to binder (W/B) ratio. Adding an internal curing agent, i.e., superabsorbent polymer (SAP), could be a viable solution in this context. However, employing SAP (without adding additional water) may also influence the fresh properties of LC3 composites by increasing yield stress and viscosity, which may be beneficial for 3D printability. Therefore, this study attempts to use SAP as a rheology modifying admixture with the aim of investigating the impact of SAP on flow behavior, structural build-up, hydration kinetics, compressive strength, and autogenous shrinkage of LC3 pastes with a fixed W/B (0.3). In addition, hydroxypropyl methylcellulose (a typical rheology/viscosity modifier in 3D printable cementitious materials) was also employed in two mixtures to compare their effects. Results show that adding SAP increases the dynamic yield stress and the apparent viscosity, as well as structural build-up and hydration, but decreases the compressive strength at 3, 7 and 28 days. Furthermore, using SAP (especially 0.2 wt % SAP) not only promotes the early-age expansion but also effectively mitigates the autogenous shrinkage of LC3 pastes for up to 7 days. Overall, the obtained results indicated that SAP could act as a promising rheology modifier for the development of 3D printable cementitious materials.

1. Introduction

Substituting part of Portland cement (PC) or clinker with supplementary cementitious materials (SCMs) for making blended cement is a sustainable strategy to reduce the carbon footprint of the cement industry [1]. However, the most commonly used SCMs, i.e., fly ash and slag, are gradually declining in availability [2–4], hindering the application of blended cement. Increasingly, limestone and calcined clay are proposed as alternatives to SCMs due to their abundant deposits and supply worldwide [2,5]. Limestone-calcined clay-cement (LC3), comprised of up to 50% blend of calcined kaolinitic clay and limestone, was proposed as one of the most promising sustainable cements and has been under development in the last decade [2,6]. LC3 can provide comparable compressive strength to PC from 7 days onwards [7] and displays good durability, e.g., excellent resistance to chloride penetration [8,9] and alkali-silica reaction (ASR) [10]. Furthermore, producing 1 ton of LC3 may reduce the CO_2 emissions by up to 40% compared to PC [11].

Early-age cracking caused by volumetric reduction is a critical issue for the health of concrete structures, severely affecting mechanical performance, and long-term durability [12,13]. Autogenous deformation is one of the prominent reasons for volume change of cementitious materials occurring after forming a solid skeleton. In particular, when the water-to-cement (or binder) mass ratio (W/C or W/B) is less than 0.42, autogenous shrinkage plays a dominant role in the early-age cracking of cementitious material [14]. This is because autogenous shrinkage is driven by capillary tension generated in the process of hydration-induced self-desiccation [15]. The low W/C or W/B may result in small capillary pore size, which can induce high capillary tension according to the Laplace and Kelvin Laws. Recent studies have shown that LC3 could be used in ordinary/normal concrete, as well as high-performance concrete [16] and 3D printable cementitious materials [17-19]. According to Scrivener et al. [11], the autogenous shrinkage seems not to be an issue for the use of LC3 in ordinary/normal

* Corresponding author.
E-mail addresses: Y.Chen-6@tudelft.nl (Y. Chen), M.Liang-1@tudelft.nl (M. Liang), Y.Zhang-28@tudelft.nl (Y. Zhang), Z.Li-2@tudelft.nl (Z. Li), B.Savija@tudelft.nl (B. Šavija), Erik.Schlangen@tudelft.nl (E. Schlangen), O.Copuroglu@tudelft.nl (O. Çopuroğlu).

https://doi.org/10.1016/j.conbuildmat.2023.130777
Received 11 August 2022; Received in revised form 19 December 2022; Accepted 16 February 2023
Available online 22 February 2023

concrete (W/B = 0.4). The authors found that the onset of autogenous shrinkage was postponed by 4 days in LC3-50 (50% clinker, 15% limestone, 30% calcined clay, and 5% gypsum) pastes compared to PC pastes. After 28 days, LC3-50 showed a similar total autogenous shrinkage to the PC. In contrast, as reported by Hay et al. [14], higher autogenous shrinkage was observed in LC3 pastes in comparison with PC pastes when the W/B was 0.485. Nguyen et al. [12] found that LC3 concrete (0.4 of W/B) showed a much more pronounced autogenous shrinkage than PC concrete at later age (up to 100 days) probably due to the pore refinement. Different findings in this regard may be governed by the variation in the composition of calcined clay, sulfate content and time zero selection. Additionally, for most of high-performance concrete and 3D printable cementitious materials, a relatively low W/B (e.g., equal to or less than 0.35) is typically employed, which may cause a particularly significant autogenous shrinkage [20]. Du and Pang [16] reported that autogenous shrinkage of LC3 paste with a W/B of 0.3 increased with limestone and calcined clay contents and was much higher than that of PC paste in the first 10 days.

Internal curing is a commonly accepted approach for maintaining high internal relative humidity (RH), and mitigating the autogenous shrinkage during hydration of cementitious materials [21,22]. Superabsorbent polymer (SAP), as one of the most efficient internal curing agents for cementitious materials, has been widely studied and reported. Due to the cross-linked polyelectrolytes with hydrophilic network structures, SAP can physically absorb water or solutions and then release them to balance the internal RH [23]. However, to our knowledge, few studies have attempted to use SAP in LC3-based cementitious materials to prevent the early-age cracking induced by autogenous shrinkage. Besides, due to the water absorption of SAP, the fresh-state behavior of cementitious materials may be modified by the addition of SAP. Snoeck et al. [24] found that the flowability of PC mortar can be significantly decreased by adding SAP. Additional water seems to be needed to retain the fluidity of fresh mortar [24,25], while excess water may be added due to the overestimation of the initial absorbency [26]. In addition to increasing water amount, some studies kept the same water content but adjusted the flowability by increasing superplasticizer dosage [27–29]. For the flow behaviors of fresh cementitious materials, rheological indicators, including yield stress and plastic viscosity, can be modified using SAP [30–32]. Owing to the unique physical features of calcined clay, i.e., high specific surface area (SSA), small particle size, and layered particle structure [33–35], the impacts of SAP on fresh properties (e.g., flow behavior and structural-build up) of LC3 may be more significant than PC or other blended cements. On the other hand, the increase in yield stress and viscosity of fresh cementitious materials induced by SAP may be beneficial for improving 3D printability. In this context, SAP may play the same role as viscosity/rheology modifying admixture (VMA) used in many 3D printable cementitious materials [19,36,37]. Nevertheless, few studies have attempted to employ SAP as a VMA.

Moreover, the hydration and mechanical performance of hardened cementitious materials can be severely influenced by the addition of SAP. According to earlier investigations [38,39], the formation of C-S-H gel may be promoted by internal curing ascribed to the desorption of SAP. Meanwhile, macro-voids/cavities form as a result of water release from SAP, thereby reducing the strength of cementitious matrix [24,40]. Nevertheless, these impacts of SAP may also depend on the binder composition, and it is therefore unclear what the effects would be for LC3 mixtures with a relatively low W/B (e.g., 0.3).

This study attempts to employ SAP as a rheology modifier with the aim of investigating the impact of SAP on flow behavior, structural build-up, hydration kinetics, compressive strength, and autogenous shrinkage of LC3 pastes with a fixed W/B (0.3). Hydroxypropyl methylcellulose, as a typical VMA used in 3D printable cementitious materials, was also employed in two mixtures to compare the effects caused by SAP. The rheological behavior of fresh pastes was characterized using flow curve, amplitude sweep, and small amplitude oscillatory shear tests. Furthermore, isothermal calorimetry and thermogravimetric analysis (TGA) were carried out to determine the hydration of mixtures with SAP and/or VMA. Compressive strength of paste samples was measured at 3, 7, and 28 days. The air void content of hardened samples was quantified using X-ray computed tomography (CT) scanning and image analysis. Additionally, linear autogenous shrinkage of studied mixtures was quantified using the corrugated tube test method.

2. Material and methods

2.1. Materials

The binding materials used in this study included CEM I 52.5 Portland cement (PC), calcined clay (CC), limestone powder (LP), and gypsum. Calcined clay with about 50% of metakaolin was provided by Argeco, France. Gypsum with more than 99% purity was purchased from Merck KGaA, Germany. Fig. 1 (a) illustrates particle size distribution of all fines. Calcined clay had the coarsest grain size compared to other binding materials. X-ray diffraction (XRD) patterns of PC, CC, and LP (PhilipsPW1830 powder X-ray diffractometer with Cu-Kα radiation) are reported in Fig. 1 (b). Quartz was the major impurity in the calcined clay used. The reactive silica and aluminate contents in the calcined clay are 12.3 wt% and 32.0 wt%, respectively. X-ray fluorescence (XRF) characteristics of PC, CC, and LP are presented in Table 1. Table 2 reports physical characteristics, i.e., Brunauer-Emmett-Telle (BET) specific surface area (SSA), density, and average grain size of all binding materials.

Table 3 shows that all studied paste mixtures had the same binder composition and water-to-binder mass ratio (0.3). The binder was comprised of 54 wt% PC, 30 wt% CC, 15 wt% LP and 1 wt% gypsum. Except for mixture A3, 0.8 wt% of polycarboxylate ether (PCE)-based superplasticizer (SP) (MasterGlenium®51, BASF, Netherlands) was added. A commercially available superabsorbent polymer (SAP, FLOSET 27CC, SNF Floerger, France) was employed with 0.1 wt% or 0.2 wt% in mixtures A1, A2, A3, and B2. As reported by [41], the average particle size of this dry SAP (measured by laser diffraction) is about 250 μm. As shown in Fig. 2, the absorption capacity of SAP in different types of mixing liquids was compared using a teabag method (detailed procedures given in [42,43]). It can be found that increasing SP concentration in the mixing liquid decreased the absorbed solution amount of SAP, which was consistent with the findings of [44]. Note that this study only focused on the effect of low amounts of SAPs on rheology, hydration, and compressive strength of cementitious materials. The use of high amounts of SAPs (e.g., 0.6–1 wt% of binder or cement) may cause many different phenomena and may require additional water, which can be referred to earlier studies [24,27]. In addition to SAP, 0.1 wt% of hydroxypropyl methylcellulose (HPMC)-based viscosity modifying admixture (VMA) was included in mixtures B1 and B2. This VMA was supplied by Shanghai Ying Jia Industrial Development Co., Ltd and its viscosity is about 201,000 mPa.s. A small planetary HOBART mixer was used to prepare paste samples. The mixing liquid (water + SP) was added to the binder in a bowl and mixed at low and high speeds for 2 min and 1.5 min, respectively.

2.2. Test procedures

2.2.1. Rheological tests

Rheological behaviors of studied mixtures were characterized using an Anton Paar MCR 302e rheometer equipped with a cylindrical measuring cell (28.92 mm inner diameter and 68 mm depth) and a four-blade vane (22 mm diameter and 40 mm height). The inner surface of the measuring cell was fitted with steel lamellas to mitigate slippage. About 88 g of fresh paste was filled in the measuring cell for each measurement. Prior to testing, the fresh mixture was compacted using a vibration table (30 Hz for 30 s) to minimize the entrapped air voids. Before conducting rheological tests, 100 s^{-1} of shear rate was executed

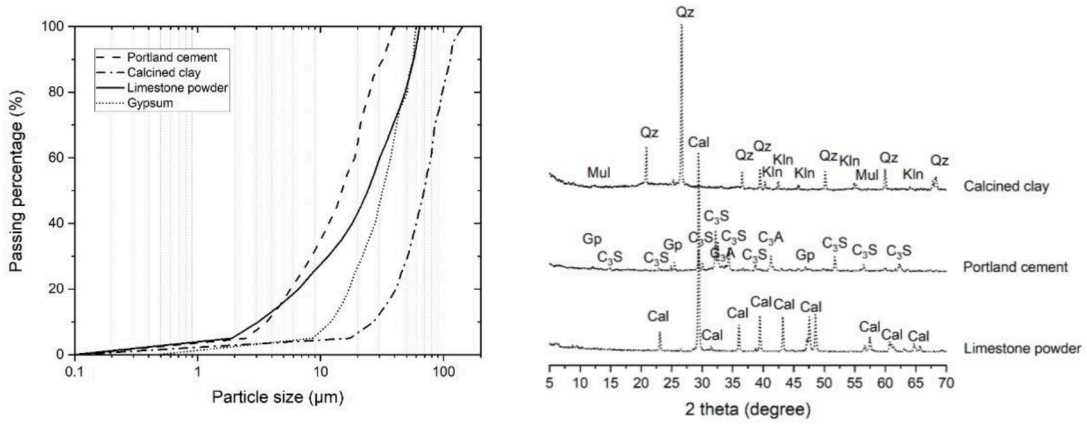

(a) (b)

Fig. 1. (a) Particle size distribution of CEM I 52.5 R Portland cement, limestone powder, calcined clay, and gypsum. (b) X-ray diffraction (Cu-Kα radiation) patterns of CEM I 52.5 R Portland cement, limestone powder, and calcined clay. Cal-calcite, Gp-gypsum, C_3S-alite, C_3A-tricalcium aluminate, Mul-mullite, Qz-quartz, Kln-kaolinite.
Adapted from [45]

Table 1
Oxide compositions of calcined clay, limestone powder, and CEM I 52.5 R Portland cement, measured using XRF [45].

XRF [wt.%]	Calcined clay	Limestone powder	Portland cement
CaO	0.55	55.40	68.71
SiO_2	55.14	0.17	17.41
Al_2O_3	38.43	0.03	4.62
Fe_2O_3	2.60	0.04	2.75
K_2O	0.17	0	0.63
TiO_2	1.12	0	0.34
ZrO_2	0.05	0	0
SO_3	0	0	2.44
Other	1.94	44.36	3.10
Total	100.00	100.00	100.00

Table 2
Physical characteristics of all binding materials [45].

	Calcined clay	Limestone powder	Portland cement	Gypsum
Density [g/cm^3]	2.51	2.65	3.12	2.32
SSA [m^2/g]	10.06	1.22	1.16	0.53
D_{v50} [μm]	69.35	24.19	14.86	31.94

to the fresh sample at 7 min for 30 s to keep a similar flow history. Afterwards, a resting time of 150 s and 30 s were applied for flow curve and strain sweep tests, respectively. SAOS test was performed after strain sweep test at the material age of 22 min. All tests were conducted at room temperature (about 20 °C).

2.2.1.1. Flow curve test. Fig. 3 (a) shows the protocol of the flow curve test used in this study. For each sample, three testing trials were conducted at the material age of 10 min, 25 min, and 40 min. The resting time between two testing trials was 5.5 min. In the testing trial, the shear rate increased in nine consecutive steps from 10 s^{-1} to 100 s^{-1} and then decreased following the same interval from 100 s^{-1} to 10 s^{-1}. The increasing shear rate part was employed to ensure a deflocculated state of fresh paste, and the decreasing regime was used to obtain the flow behavior. Each shear rate needed 30 s to reach the steady flow regime, resulting in 9.5 min total time for each trial. The data was collected every 0.3 s. Fig. 3 (b) illustrates the typical flow curve of one testing trial. The last 30 measuring points, providing an equilibrium value, were averaged to represent the shear stress at the given shear rate. The

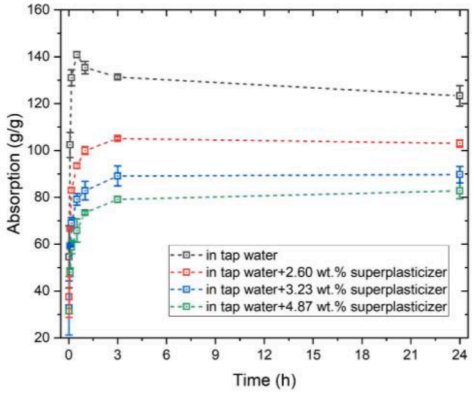

Fig. 2. Absorption capacity of the SAP in tap water, mixing liquids (tap water + 2.60 wt%, 3.23 wt%, and 4.87 wt% superplasticizers) using the teabag method. 2.60 wt% and 3.23 wt% of superplasticizers in mixing liquids are equivalent to 0.8 wt% and 1 wt% of superplasticizers in the binder.

Table 3
Mix designs of cementitious materials (% of the binder mass).

	Portland cement [wt.%]	Limestone powder [wt.%]	Calcined clay [wt.%]	Gypsum [wt.%]	Water [wt.%]	SP [wt.%]	SAP [wt.%]	VMA [wt.%]
REF	54	15	30	1	30	0.8	0	0
A1	54	15	30	1	30	0.8	0.1	0
A2	54	15	30	1	30	0.8	0.2	0
A3	54	15	30	1	30	1	0.2	0
B1	54	15	30	1	30	0.8	0	0.1
B2	54	15	30	1	30	0.8	0.1	0.1

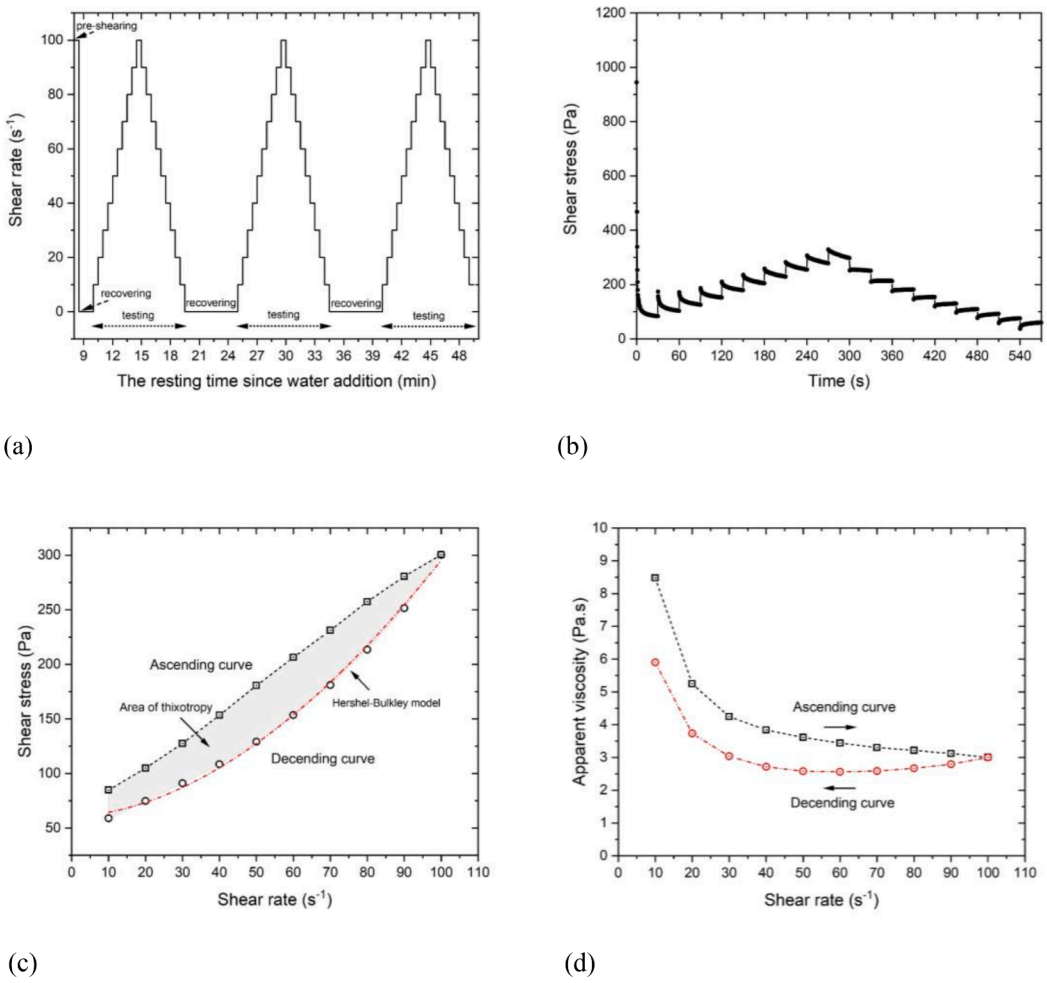

Fig. 3. (a) Protocol of flow curve test (at material ages of 10 min, 25 min, and 40 min) used in the study. (b) A typical flow curve of one testing trial. (c) The average shear stresses with various shear rates. The descending curve was fitted using the Hershel-Bulkley model. (d) The average apparent viscosity at different shear rates.

obtained shear stresses at different shear rates are plotted in Fig. 3 (c). The area of up and down curves was considered to indicate the thixotropic behavior of the tested material. Moreover, the descending curve of all studied mixtures followed the Herschel-Bulkley model (Eq. (1)) and was used to determine the dynamic yield stress.

$$\tau = \tau_0 + k\dot{\gamma}^n \tag{1}$$

where τ_0 and $\dot{\gamma}$ are dynamic yield stress and shear rate. k and n denote consistency factor and power index. The apparent viscosity η at each shear rate in Fig. 3 (d) can be computed using Eq. (2).

$$\eta = \tau(\dot{\gamma})/\dot{\gamma} \tag{2}$$

2.2.1.2. Oscillatory shear test. After 30 s of pre-shearing and 30 s of recovering, the amplitude sweep test with the strain of 0.0005%–50% and a frequency of 1 Hz was applied at the material age of 8 min. The test duration was about 14 min. The linear viscoelastic domain (LVED) of studied mixtures can be determined by this manner, and the critical strain was defined as the maximum strain of LVED.

Small/low amplitude oscillatory shear test, as a non-destructive measurement, was employed to quantify the structural evolution of fresh pastes with viscoelastic behaviors. As shown in Fig. 4, a continuous sinusoidal oscillatory strain γ that is smaller than the critical strain is applied to the fresh sample.

$$\gamma = \gamma_0 \sin\omega t \tag{3}$$

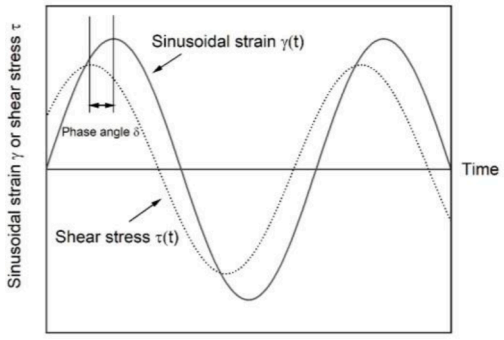

Fig. 4. Illustration of applied sinusoidal strain $\gamma(t)$ and measured response (shear stress) $\tau(t)$ for a typical viscoelastic material in the SAOS test. Adapted from [54]

where γ_0 means maximum strain amplitude. ω and t represent the constant frequency and time. In this study, 0.005% of the maximum strain amplitude was employed according to the test results of amplitude sweep in Section 3.2.1. Such a strain also agrees with the values reported by earlier studies [46–50]. In addition, for fresh cementitious materials, the measured storage modulus using the oscillatory shear test is independent of the frequency when the applied frequency is larger than 0.2 Hz [51]. 1 Hz of frequency employed by [52,53] was selected in the current work. The measured response (shear stress) as a function of time

can be presented as:

$$\tau(t) = \gamma_0(G'\sin\omega t + G''\cos\omega t) \quad (4)$$

where G' is storage modulus indicating the elastic or in-phase component of stress. G'' is loss modulus representing the liquid, viscous, or out-of-phase component of stress. Additionally, the ratio between G'' and G' is defined as loss factor ($\tan(\delta)$) that was used to indicate the lag between the applied strain and the resulting stress [51].

$$\tan\delta = G''/G' \quad (5)$$

δ denotes the phase angle. The material displays solid state behavior when the loss factor is close to zero. In contrast, a viscous/liquid-like state can be determined.

2.2.2. Characterization of hardened properties

The hydration heat released for the first 7 days was measured by an eight-channel TAM Air isothermal calorimeter. After mixing the pre-weighed dry components with the pre-mixed liquid (water and SP) by a mixing machine for 3 min, 6 g of fresh paste was filled into a 20 mL glass vessel. The glass vessel, together with a reference vessel that was filled with fine quartz sand, were sealed and placed in the calorimeter under 20 °C. Heat values were recorded each 30 s. In addition, TGA was also used to quantify the effect of chemical additives on hydration. The hydration of studied mixtures was stopped using solvent exchange method with isopropanol (procedures were referred to [18,55]) at the material age of 1 and 7 days. About 50 mg of powder sample was heated from 40 to 900 °C (heating rate: 10 °C/min) and the test was in an argon environment with a 30 mL/min flow rate.

Compressive strength of mold-cast paste samples (40 mm cubic specimens) was tested at 3, 7 and 28 days. All specimens were cured and stored in sealed plastic bags under an ambient temperature of about 20 °C. According to NEN-EN 196-1 [56], 2.4 kN/s of loading rate was chosen for compressive strength testing. The compressive strength of each mixture at each age was obtained by three repeated tests. The air void analysis of studied mixtures was conducted using CT scanning and image analysis through ImageJ (open-source software). Details can be found in our earlier studies [19,57]. Cylindrical samples (25 mm diameter and 20 mm height) were casted by using cylindrical plastic mold. A spatial resolution of 15 μm^3/voxel was obtained. A rectangle region of interest (ROI) with a side length of 17 mm was extracted from the image stack to perform the image analysis. For every sample, 700 transverse planes (grayscale images) were employed. Note that only the size of air voids larger than 15 μm can be considered.

Additionally, an automatic Vicat test apparatus was used to measure the initial and final setting times of studied mixtures. The test was performed by following NEN-EN 196-3 [58]. Note that the initial setting time in this study was defined as the time elapsed between the time of adding water and the time at which the penetration depth was 36 mm. For the final setting time, the penetration depth was about 5 mm (the needle without attachment). The linear autogenous shrinkage was quantified using paste samples according to ASTM C1698-19 [59]. Corrugated tubes (28.5 mm diameter and 425 mm length) were utilized, and the deformation of each specimen was automatically measured using linear variable differential transformers (LVDTs) until 7 days.

3. Results and discussion

3.1. Flow curves

The average shear stresses at the different shear rates from the descending part of flow curve were fitted by the Herschel-Bulkley model, as shown in Fig. 5 (a) (b). The obtained dynamic yield stress and power index are presented in Fig. 5 (c) (d). For mixtures REF, A1 and A2, increasing SAP content increased shear stress at the same shear rate and dynamic yield stress at the same material age. The enhancement in yield stress can be ascribed to the reduction of free water in the cementitious material due to the water absorption of SAP [30]. Compared to mixture A2, mixture A3 with a slightly higher SP dosage showed lower dynamic yield stress. However, the water uptake was significantly decreased by increasing the concentration of SP. There appeared to be more free water in mixture A3 (see Fig. 2), resulting in lower yield stress. The dynamic yield stress was significantly increased by adding VMA, especially when the SAP was also added (mixture B2). This is because HPMC-based VMA can not only physically absorb large amounts of free water through forming the hydroxyl bonds, but can also enhance the flocculation between cementitious particles via different mechanisms, i.e., bridging flocculation (adsorbing cementitious particles), polymer–polymer interaction and entanglement [60,61]. Mixtures B1 and B2 showed higher dynamic yield stress at 25 min than at 10 and 40 min, whereas the dynamic yield stress of mixtures REF, A1, A2, and A3 was relatively constant within the first 40 min. The fluctuation of dynamic yield stress for mixtures B1 and B2 may be tied to the competitive adsorption between VMA and SP molecules, resulting in the presence of non-adsorbing polymers in the fresh mixture. Attractive depletion forces caused by these non-adsorbing polymers [62] may lead to the instability of yield stress of the suspension.

A shear thickening behavior of mixtures REF, A1, A2, and A3 was observed since the power index was higher than 1 (Fig. 5 (d)). Conversely, using VMA resulted in a shear-thinning behavior. The average apparent viscosity can also confirm the shear-thinning or thickening behavior at the different shear rates in Fig. 5 (e) (f). After a sharp decrease (shear rate: 10–40 s^{-1}), the apparent viscosity of mixtures REF, A1, A2, and A3 increased slightly with the shear rate. In contrast, a continuous decrease in apparent viscosity was found in mixtures B1 and B2. According to Roussel et al. [63], the shear thickening behavior at the relatively high shear rate may be governed by the inertial effects and solid contacts between cementitious particles. As reported by [64], the use of calcined clay can reduce the average interparticle distance between particles, thereby promoting their solid contacts. This behavior cannot be modified by only adding 0.1–0.2 wt% SAP but can be altered by adding 0.1 wt% VMA. Except for the water retention property, the use of VMA can also increase the cohesion and macroscopic viscosity of cement suspension [60], which may extend the viscous regime. Consequently, the applied shear rate (up to 100 s^{-1}) was insufficient to reach the inertial regime in this context.

Fig. 5 (g) compares the thixotropic area of different mixtures at 10 min. Note that the thixotropy in this context was only used to describe the reversible effect (see [47,65,66]). Thus, the area of thixotropy can represent the magnitude difference between dynamic and static states of a fresh mixture. As shown in Fig. 5 (g), the thixotropy of fresh mixtures was enhanced by increasing SAP dosage and/or adding VMA at 10 min. The increase in thixotropy by adding 0.1 wt% VMA was more significant than increasing the dosage of SAP from 0.1 wt% to 0.2 wt%, which was attributed to the flocculation enhancement of VMA, as mentioned earlier. Furthermore, increasing SP amount also increased the area of thixotropy, probably due to the attractive depletion forces induced by the presence of non-adsorbing polymer in the pore solution [67].

3.2. Structural build-up

3.2.1. Linear viscoelasticity domain and critical strain

The variation of G' determined from the amplitude sweep measurement for different studied mixtures at 8 min is presented in Fig. 6 (a). All curves showed a near-linear growth until reaching a critical strain. After the critical strain, the increase in G' became smaller, and then G' decreased after the peak. According to [49,67], G' is independent of the applied strain within the linear viscoelastic domain (LVED). Thus, the linear growth of G' within LVED is ascribed to the flocculation nature of cementitious materials at the resting time. The decrease in G' with increasing the shear strain amplitude is related to the breakage of the flocculated microstructure. Fig. 6 (b) compares the critical strain of

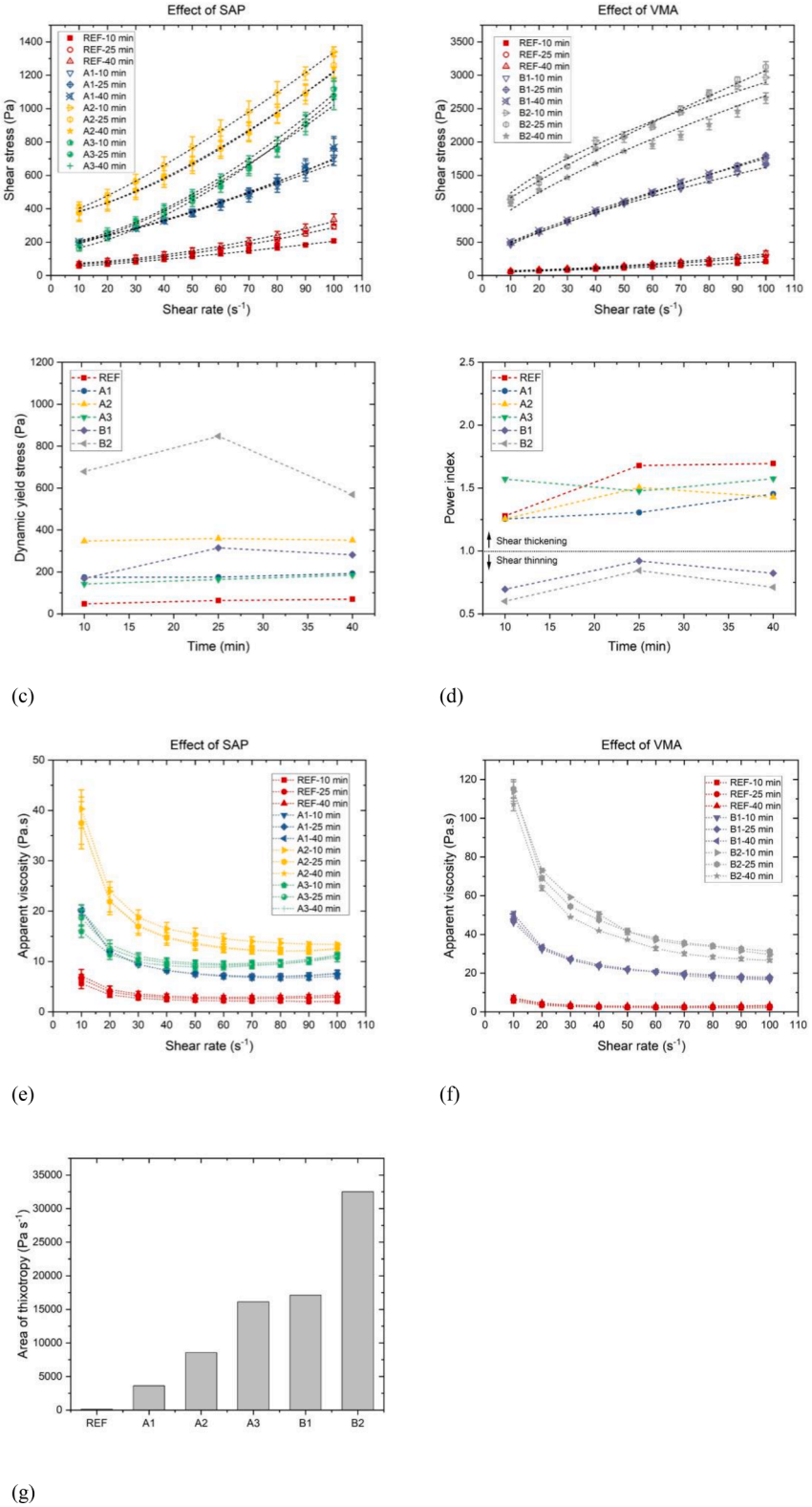

Fig. 5. Flow curves at the material ages of 10 min, 25 min, and 45 min – descending curves fitted by the Herschel-Bulkley model of (a) mixtures REF, A1, A2, and A3, and (b) mixtures REF, B1, and B2. (c) Dynamic yield stress of different mixtures. (d) Power index of different mixtures. The average apparent viscosity at different shear rates (descending part): (e) mixtures REF, A1, A2 and A3, and (f) mixtures REF, B1 and B2. (g) Area of thixotropy for different mixtures at 10 min.

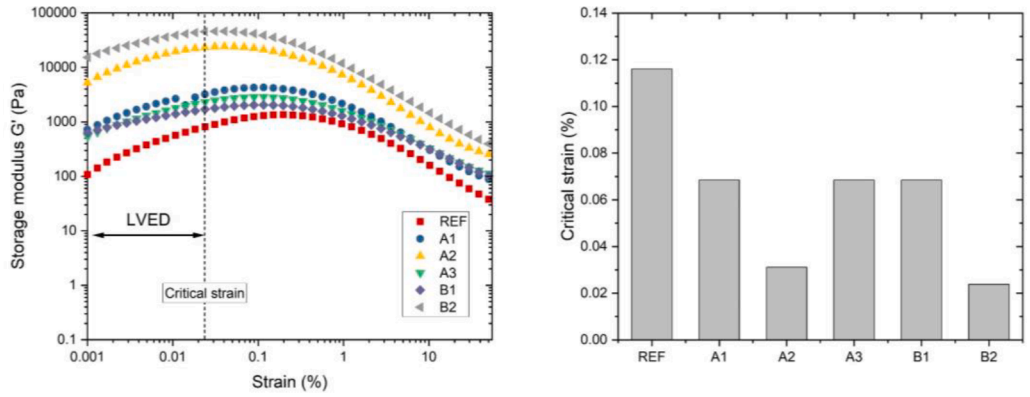

Fig. 6. Amplitude sweep test results (started at 8 min): (a) Storage modulus *G'*. (c) Critical strain of different mixtures.

different studied mixtures. The critical strain was decreased by increasing SAP dosage and/or adding VMA. Mixture B2 showed the lowest critical strain (about 0.02%) due to the use of both VMA and SAP. Compared to mixture A2, mixture A3 with a higher amount of SP displayed a more considerable critical strain. The strain amplitude used in the SAOS test should be less than 0.02% to ensure that *G'* evolution of all mixtures is not disturbed by the applied strain. Therefore, 0.005% of applied strain amplitude in the SAOS testing is suitable.

3.2.2. Structuration with time

Fig. 7 reports SAOS test results of different mixtures from 22 min to 72 min, including the evolution of storage modulus *G'*, loss modulus *G''*, and loss factor *G''/G'*. As shown in Fig. 7 (a), *G'* of mixtures REF, A1, A3, and B1 demonstrated a similar development path. *G'* showed a near-linear growth at a very small slope within the first 15–20 min, and then developed with a much higher linear evolution rate. Except for these two stages, *G'* of mixtures A2 and B2 also had a third stage with a smaller slope than the second one. In the first stage, *G'* evolved linearly at a relatively small rate, which may be attributed to the retarding effect of SP on the flocculation [68–70]. According to Roussel et al. [65], the second stage (rapid *G'* growth) can be linked to the flocculation/re-flocculation of cementitious particles, resulting in the formation of a percolated network of colloidal interactions. After that, the growth rate of *G'* became smaller. The third stage indicated the formation of a percolated rigid network attributed to the C-S-H precipitating at the pseudo-contact points between cementitious particles [65,71]. The linear evolution rate of stage 1 and stage 2 and transition time t_1 were employed to compare the *G'* development of different mixtures in Fig. 7 (a) (d) (e). The high evolution rates of both stages coincided with the short transition time, as illustrated in Fig. 7 (f). For the mixture with the same SP addition, increasing SAP dosage can significantly enhance *G'* development, i.e., induce the rise in *G'* and its evolution rate in both stages, as well as a decrease in t_1. Such an enhancement in *G'* evolution can be linked to the water absorption of SAP, which essentially reduced the free/excess water amount, resulting in a decrease of mean inter-particle distance/water film thickness in the fresh mixture. According to [64,72], the flocculation and nucleation can be stimulated by diminishing the mean interparticle distance/water film thickness. Compared to the REF mixture, only adding 0.1 wt% VMA (mixture B1) or increasing SP percentage (mixture A3) inhibited the *G'* growth over the testing time. The former displayed more severe side effects than the latter. As reported by [67,73], a softer system (fresh mixture) with lower elastic modulus may be formed using cellulose ether-based VMA in comparison with the reference cement paste. Brumaud et al. [73] pointed out that cellulose ether adsorbed onto the surface of cement grains appeared to delay the C-S-H nucleation over the first tens of minutes after water addition. Similar to PCEs, cellulose ether adsorption could form a layer of polymer that can generate steric repulsive forces between cement grains. This effect can weaken the colloidal interaction network and adversely affect the development of rigidity. However, adding both VMA and SAP (both in 0.1 wt%) can enhance *G'* evolution, which may be governed by the synergistic effect of water absorption by both polymers. This effect still needs to be further explored.

In Fig. 7 (b), *G''* of mixtures A1, A2, and B2 increased with time until reaching a peak and then displayed a decreasing trend. The downward branch was not observed for mixtures REF, A3, and B1 because of the limited testing time. The mixtures with an earlier appearance time of the *G''* peak corresponded to a higher *G'* and a faster *G'* evolution, which agrees with results reported in [45]. Fig. 7 (c) compares the loss factor development of various mixtures. It can be found that the loss factor of mixtures A2, B1, and B2 displayed a decreasing trend with time, which indicates the forming process of a percolated rigid network between cementitious particles. A very similar value was observed between mixtures A2 and B2, which was much lower than that of mixture B1. For mixtures REF, A1, and A3, the loss factor vs. time curve exhibited the same pattern that had a peak at 30–40 min (after a short decrease process). According to earlier studies [46,74], this peak may be attributed to gelation. The solid dissolution was slightly faster than the liquid consumption, forming a relatively large volume of gel-like phases. After the peak, the loss factor of these mixtures gradually decreased over time. As mentioned earlier, the cementitious mixture tends to form a more rigid microstructure with reduced loss factor. Thus, at 72 min, mixtures A2 and B2 displayed a similar rigidity degree that was higher than other mixtures. Only adding 0.1 wt% of SAP (mixture A1) can also promote the rigidity and stiffening process, whereas the use of 0.1 wt% of VMA (mixture B1) or an additional 0.2 wt% of SP (mixture A3) resulted in a delay compared to the reference mixture. As mentioned earlier, the absorbed cellulose ether and/or PCE molecules may be at the origin of repulsive steric forces leading to the retardation of rigidity.

3.3. Hydration kinetics and compressive strength

The heat flow of studied mixtures normalized by paste mass is reported in Fig. 8 (a). It can be found that there are two peaks after the acceleration period for all curves. The first one was related to the main/C_3S hydration peak, and appeared at 12–16 h. Afterwards, due to the depletion of gypsum and fast dissolution of C_3A and/or other reactive aluminate phases in calcined clay, an aluminate reaction peak [6] was observed at 16–22 h. Based on the normalized heat flow of different mixtures, the required times to the C_3S hydration peak and the slope of the acceleration period were obtained and plotted in Fig. 8 (c) and (d), respectively. Adding 0.1 wt% SAP or 0.1 wt% VMA can accelerate and

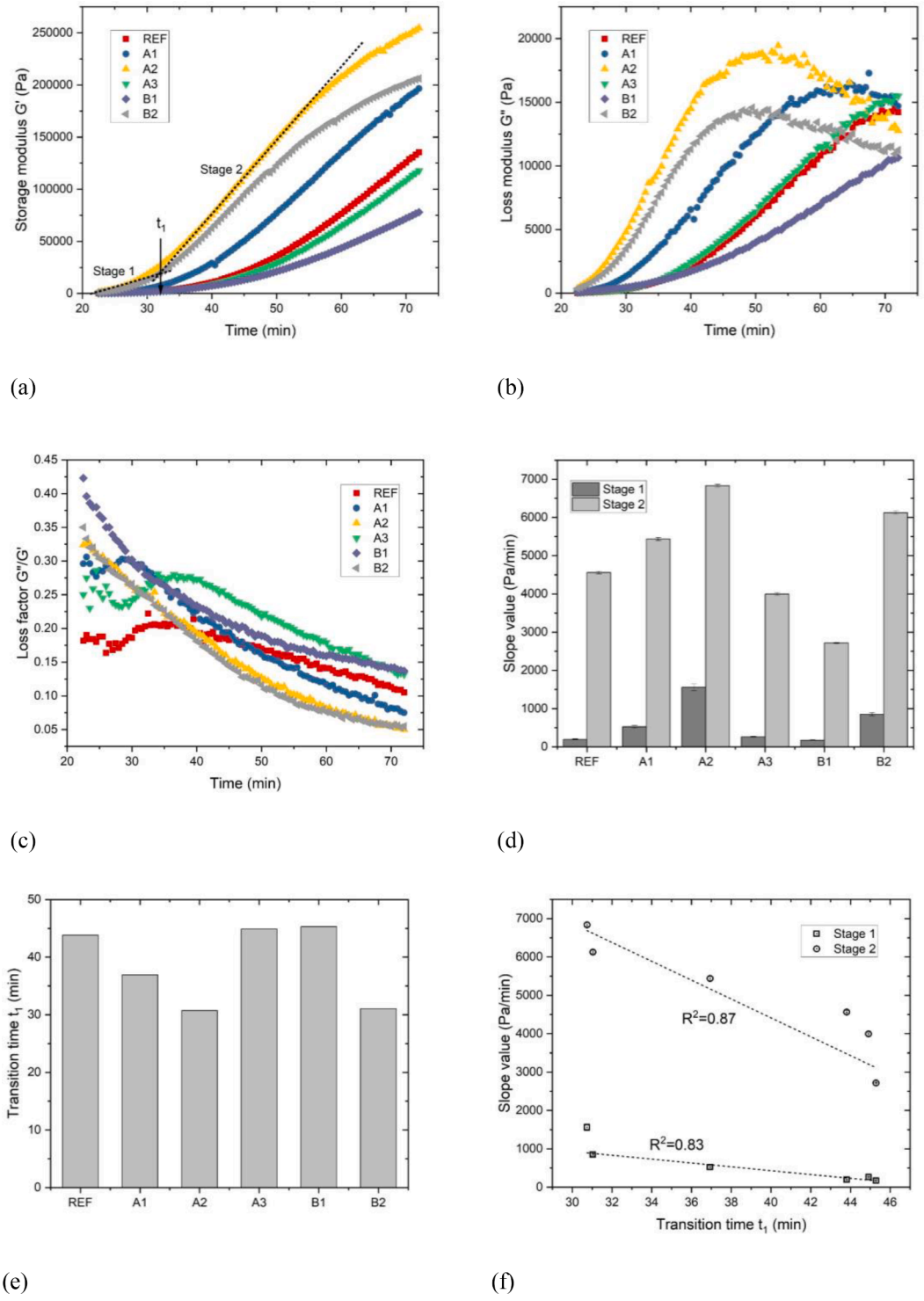

Fig. 7. SAOS test results (22–72 min): (a) Storage modulus *G'*. Two linear regimes of the SAOS curve are defined as stage 1 and stage 2. t_1 indicates the transition time between stage 1 and stage 2. (b) Loss modulus *G''*. (c) Loss factor *G''/G'*. (d) Slope value of stage 1 and stage 2. (e) Transition time between stage 1 and stage 2. (f) Correlation between slope value and transition time.

enhance the LC3 hydration. Mixtures A1 and B1 showed shorter times to reach the main hydration peak, the higher slope of the acceleration period and the intensity of C_3S peak. Increasing the amount of SAP from 0.1 wt% to 0.2 wt% can still reduce the appearance time of the main hydration peak but results in a slight decrease in the intensity of C_3S peak and the slope of the acceleration period. Similarly, the first day hydration of mixture B2 was delayed and reduced by adding 0.1 wt% SAP compared to mixture B1. This may be due to the severe water uptake of internal curing agents (0.2 wt% SAP or 0.1 wt% SAP + 0.1 wt % VMA), resulting in a significant increase in viscosity and agglomeration of cementitious particles. However, this hypothesis still needs to be confirmed by further investigation. Furthermore, increasing SP dosage can further delay the C_3S hydration, which is consistent with findings of Ref. [17].

Fig. 8 (b) reports the normalized cumulative heat of different mixtures by paste mass over the first 7 days. Adding SAP and/or VMA

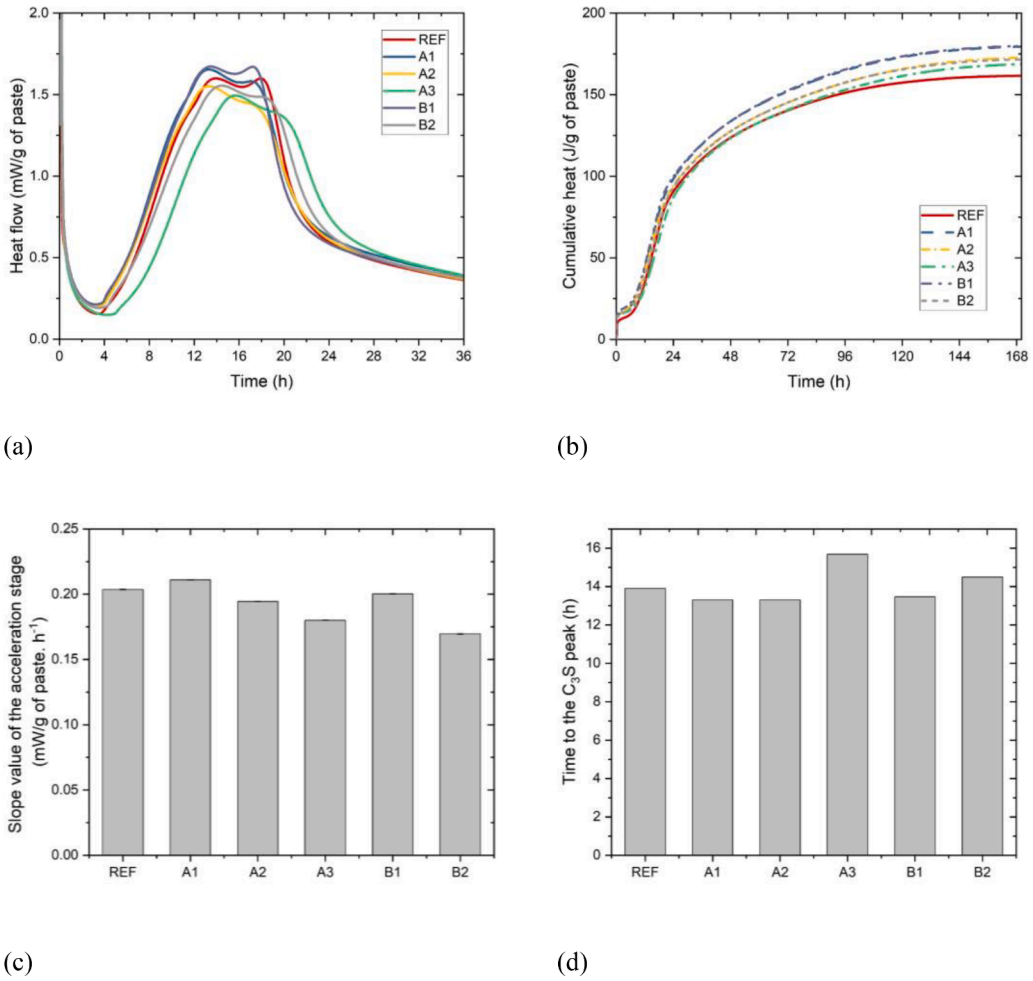

Fig. 8. Isothermal calorimetry test results: (a) Normalized heat flow by weight of paste with time (36 h). (b) Normalized cumulative heat by weight of paste with time (168 h). (c) The required time to the C_3S hydration peak of different mixtures. (d) The slope of the acceleration period of different mixtures.

resulted in a higher cumulative hydration heat than that of the REF mixture. This may be caused by the internal curing effect of these admixtures [39,75]. The release of internal curing water from SAP and/or VMA contributed to increasing the hydration degree of LC3 mixtures. However, the cumulative heat of mixtures A2 and B2 is lower than that of mixtures A1 and B1. As mentioned earlier, the particle agglomeration induced by adding high content of internal curing agent may be the main reason for reducing cumulative heat. In addition, as shown in Fig. 8 (a), the aluminate reaction appeared to be inhibited in mixtures A2 and B2, which can also cause lower heat values. Compared with the REF mixture, the cumulative heat of mixture A3 from 12 h to 48 h was slightly lower due to the delayed hydration on the first day caused by SP, but the value was higher after 72 h, which may still be related to the internal curing of SAP.

Thermogravimetric (TG) and derivative thermogravimetric (DTG) results of studied mixtures at 1 and 7 days are reported in Fig. 9 (a) (b). It can be found that a large peak appeared at 100–150 °C in DTG curves indicated water loss of C-S-H and ettringite [76]. Afterwards, a small peak at 150–200 °C (only at 7 days) revealed the decomposition of monocarboaluminate (CO_3-AFm), according to [55]. The formation of CO_3-AFm was attributed to the reaction between portlandite (CH), calcined clay and limestone [77]. The decomposition temperature of CH was in the range of 400–500 °C and the CH amount can be calculated using Eq. (6).

$$W_{[Ca(OH)_2]} = \frac{M_{400^\circ C} - M_{500^\circ C}}{M_{600^\circ C}} \times \frac{m_{[Ca(OH)_2]}}{m_{[H_2O]}} \times 100(\%) \quad (6)$$

where $W_{[Ca(OH)_2]}$ is the mass percentage of CH in mixtures. $m_{[Ca(OH)_2]}$, and $m_{[H_2O]}$ represent the molar masses of portlandite (74 g/mol) and water (18 g/mol). $M_{400^\circ C}$, $M_{500^\circ C}$ and $M_{600^\circ C}$ mean the mass percentages at 400 °C, 500 °C, and 600 °C. Fig. 9 (c) summarizes the CH content of different mixtures at 1 and 7 days. Mixture A3 exhibited a lower CH content than the reference mixture on the first day, due to the delayed C_3S hydration caused by increasing SP dosage, which is also consistent with isothermal calorimetry results. Both SAP and VMA can promote CH precipitation in the first 7 days. Increased SAP dosage enhanced CH formation at 7 days. As mentioned earlier, increasing the SAP content improved the internal curing and thus the degree of hydration. VMA has a stronger promoting effect on CH compared to SAP. CH content in mixtures B1 and B2 was higher than mixtures A1 and A2 at 7 days. The enhancement of CH formation by small amounts of VMA was also reported by Chaves Figueiredo et al. [75]. The authors attributed this CH increase to the internal curing effect of VMA.

The compressive strength of paste samples at 3, 7, and 28 days is reported in Fig. 10. Fig. 11 shows the air void analysis of different studied mixtures. Adding SAP and/or VMA negatively affected the compressive strength development. For mixtures REF, A1 and A2, increasing SAP content decreased the compressive strength up to 18%. As shown in Fig. 11 (b), the decrease in compressive strength was attributed to the increase in air void content. Two types of pores were observed in Fig. 11 (a), round bubbles (circularity = 0.8–1) and granular macro-pores (circularity = 0–0.8). The increase in SAP dosage did not increase the content of round bubbles but increased granular macro-

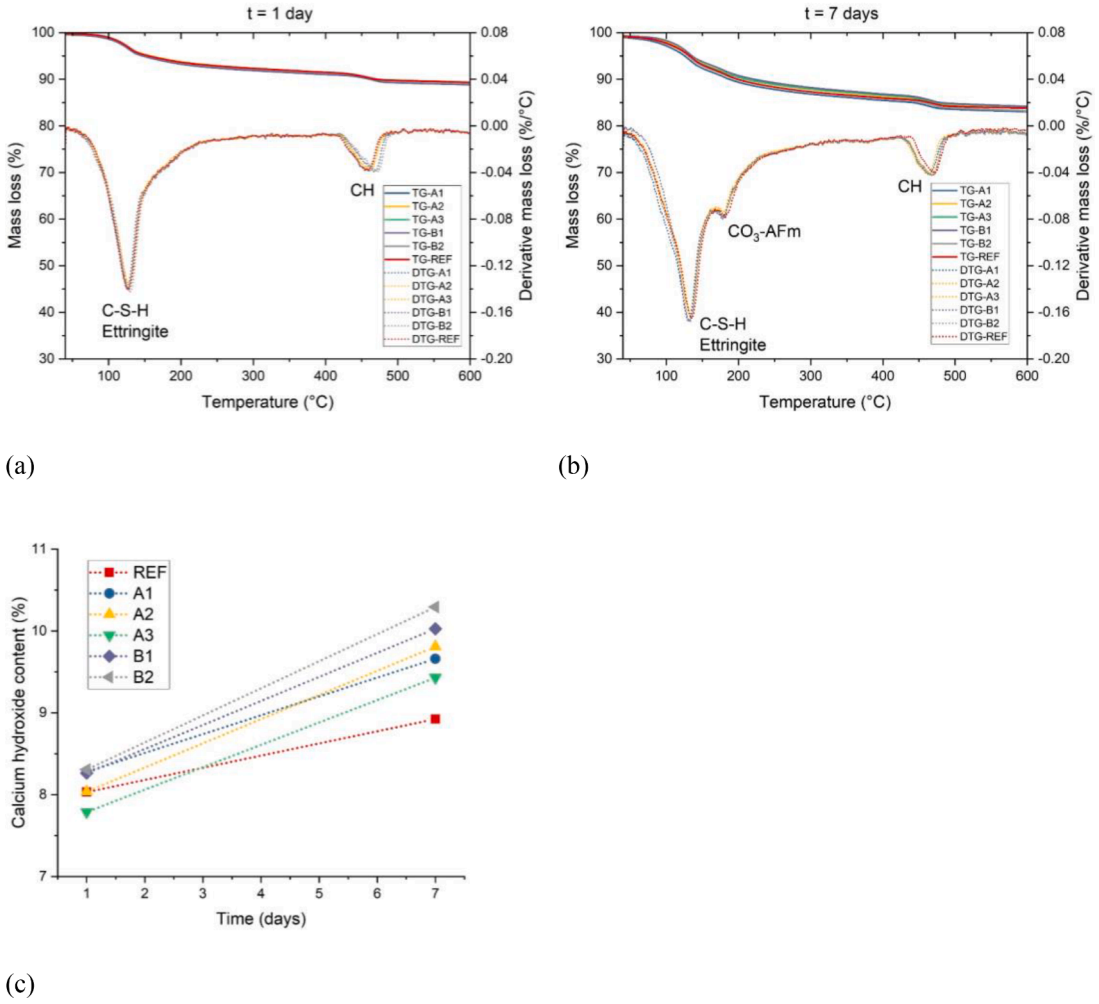

Fig. 9. TGA results: (a) TG and DTG curves of different mixtures at 1 day. (b) TG and DTG curves of different mixtures at 7 days. CO_3-AFm - monocarboaluminate, CH - calcium hydroxide/portlandite. (c) The content of portlandite normalized by the dry sample mass at 600 °C.

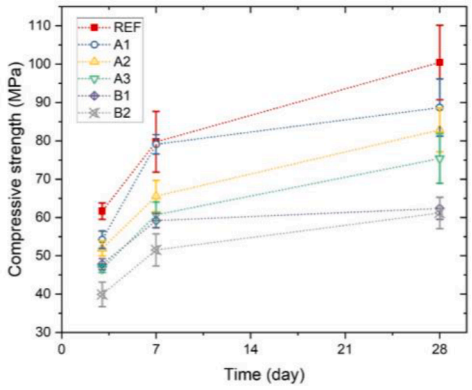

Fig. 10. Compressive strength of different mixtures at 3, 7, and 28 days.

pores (Fig. 11 (b)). The macro-pores with granular shape can be ascribed to the cavities caused by SAP and entrapped air voids due to poor workability. However, it is difficult to distinguish them based on pore size and shape. The compressive strength at all tested ages was further reduced by about 7% with increasing the dosage of SP. Compared to mixture A2, mixture A3 displayed a slightly lower air void content in Fig. 11 (b). The workability was improved by the additional SP, which reduced the entrapped air void content. Thus, the reduction of compressive strength appeared to be determined by the negative effect of SP on cement hydration (see Figs. 8 and 9).

Compared to SAP, a more significant strength reduction was found in mixtures containing VMA. As shown in Fig. 11 (a), mixtures B1 and B2 exhibited a porous matrix structure compared to other mixtures without VMA. The cohesion of fresh mixtures was significantly increased by adding VMA, potentially stabilizing many entrapped air bubbles (macro-pores) during the mixing and casting [19,75]. Additionally, the air bubbles caused by grinding aid (that is used in the production of PC) and PCE-based SP can also be stabilized in the matrix, resulting in a very porous structure. This can be evidently observed in Fig. 11 (c). Mixtures B1 and B2 contained more small air voids (0–100 μm of pore diameter) and number of pores than other mixtures. These small air voids led to the formation of a porous matrix structure that significantly weakened the compressive strength. Thus, entrapped air bubbles would be more prevalent in mixtures with VMA. Mixture B2 showed the weakest compressive strength at all tested ages owing to the overlapping effect of SAP and VMA on porosity.

3.4. Autogenous shrinkage

As shown in Fig. 12 (a), autogenous shrinkage (AS) of studied mixtures can be divided into 3 phases: fast chemical shrinkage, autogenous swelling, and autogenous shrinkage. Due to the low elastic modulus and high creep/relaxation [78–80], the AS can only generate a very limited

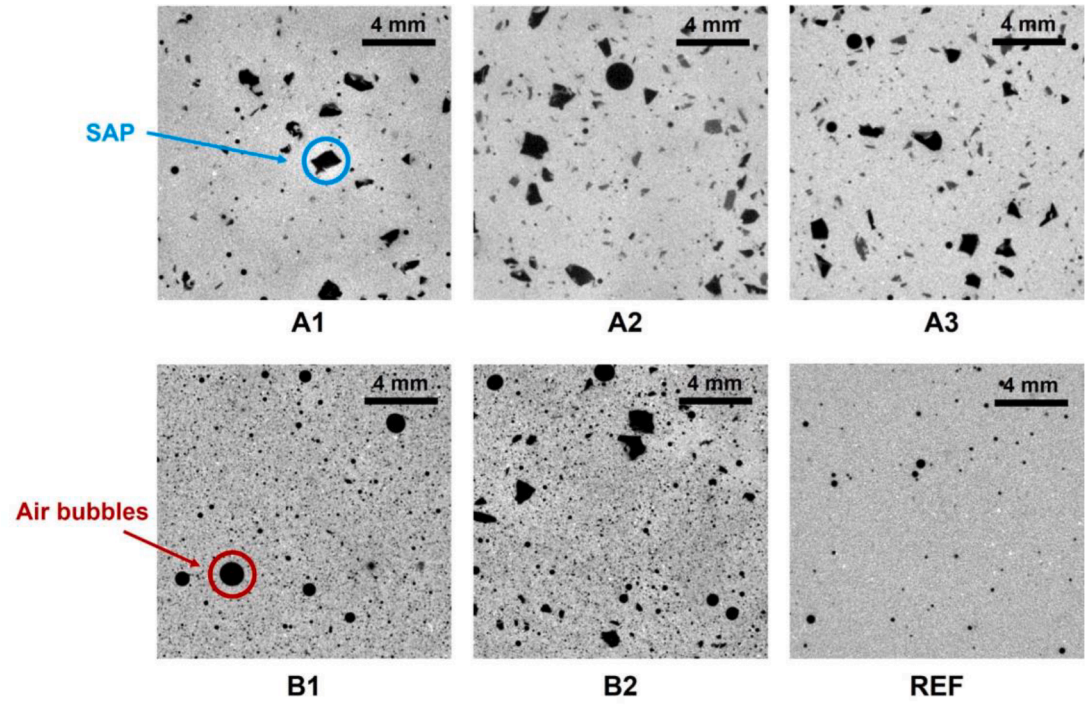

(a)

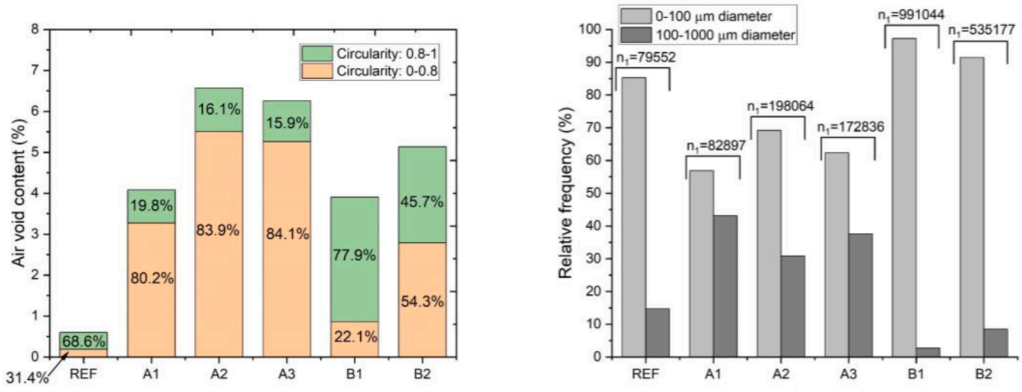

(b) (c)

Fig. 11. Air void analysis: (a) Grayscale image of different mixtures. (b) Air void content of different samples. Circularity = $4\pi(A/S^2)$, A and S are area and perimeter of the air void. (c) Relative frequency of air voids in two pore size groups (0–100 μm and 100–1000 μm of pore diameter). n_1 indicates the total number of air voids.

amount of stress in the first hours. To characterize the early-age cracking (EAC) risk, a proper selection of time-zero is essential since it denotes the onset when the AS-induced stress starts to accumulate in the restrained specimen. However, time-zero is too complex to define. Earlier studies [15,81–84] attempted to define time-zero based on AS rate peak, the onset of internal capillary pressure, relative humidity change, after early-age swelling or setting time. Considering the uncertainty of time-zero selection, this study selected 4 time-zeros of AS, as shown in Fig. 12 (b) (c) (d) (e): initial setting time, final setting time, 12 h and time of the expansion peak (after early-age swelling). The analysis for the AS with different time-zeros was presented as follows:

1) As shown in Fig. 12 (b) (c) (T_0 = initial or final setting times), the AS process for all mixtures was still governed by the chemical shrinkage at the first few hours. Adding SAP and/or VMA seemed to mitigate the AS of LC3 paste. For the mixtures incorporating SAP (A1, A2, A3, and B2), apparent expansion was observed, which compensated for the AS and was beneficial in preventing EAC since the induced compression can delay the onset of tensile stress.
2) All AS processes showed an expansion peak when the time-zero was defined as 12 h (Fig. 12 (d)). The mixtures with 0.2 wt% SAP displayed a relatively higher peak around 18 h than other mixtures. Such a peak can be ascribed to the water desorption of SAP. The magnitude of the expansion peak was enhanced by increasing SP dosage or adding 0.1 wt% VMA. After the peak, the AS of mixtures REF, A1, B1, and B2 gradually increased over time, whereas a constant value was found in mixtures A2 and A3. Furthermore, only 0.1 wt% VMA addition (mixtures B1 and B2) can also mitigate AS within the first 7 days due to the internal curing of VMA.

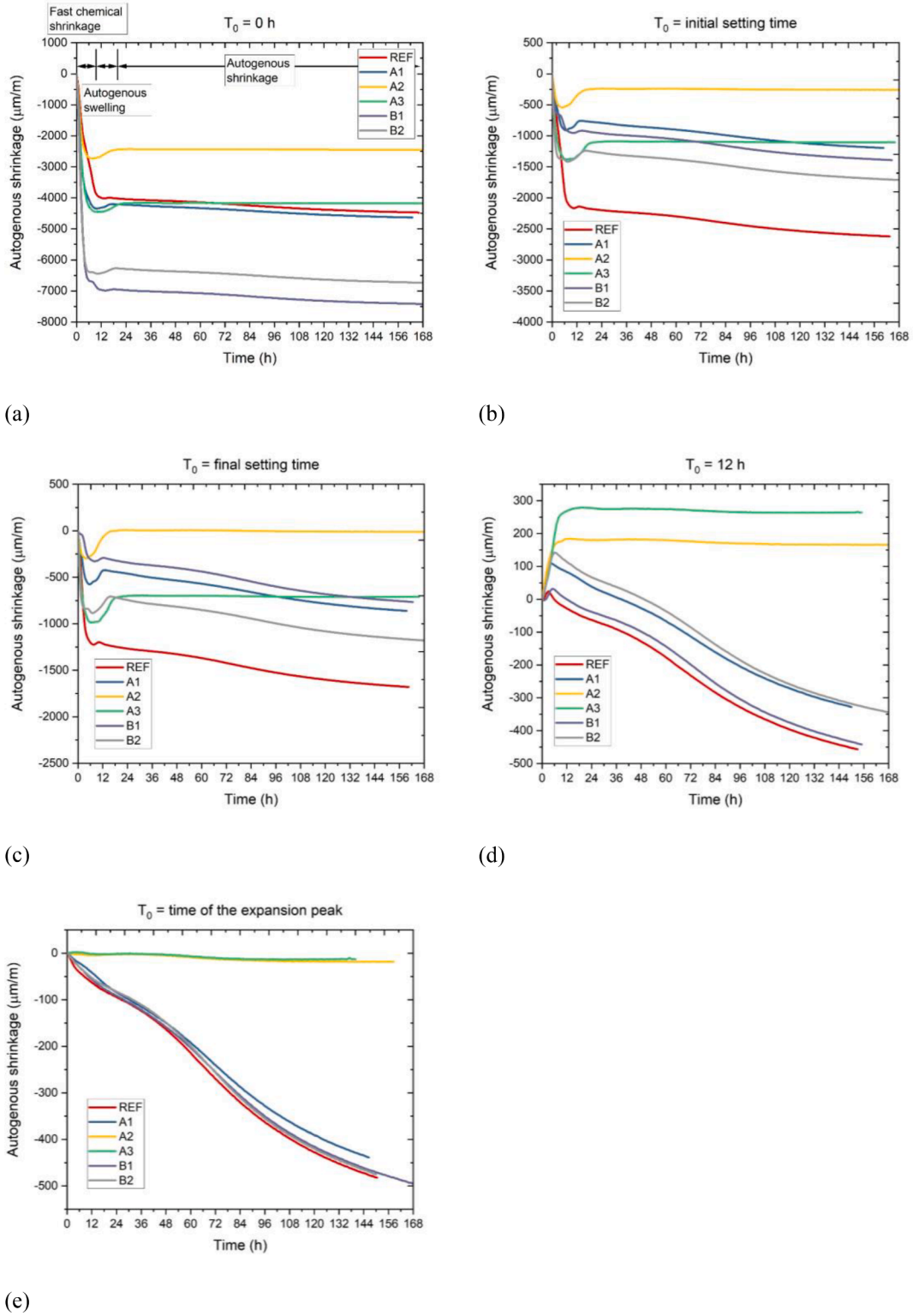

Fig. 12. Autogenous shrinkage of different mixtures: (a) time zero T_0 = 0 h (the start time of measurement); (b) time zero T_0 = initial setting time; (c) time zero T_0 = final setting time; (d) time zero T_0 = 12 h; (e) time zero T_0 = time of the expansion peak (after early-age swelling).

3) If T_0 = time of the expansion peak (after early-age swelling) (Fig. 12 (e)), mixtures A2 and A3 with 0.2 wt% SAP showed negligible AS in comparison with others, which can confirm the effectiveness of SAP in mitigating AS over the first 7 days. Also, the addition of 0.1 wt% SAP can slightly improve AS at later ages. However, limited mitigation in AS can be found by adding 0.1 wt% VMA. The use of VMA even counteracted the internal curing effects of SAP in mixture B2.

Overall, the addition of 0.2 wt% SAP not only contributed to the high expansion peak in the first few hours but also effectively reduced the AS in the later ages. Considering the occurrence of the "knee point" in Fig. 12 (d), the starting time of 12 h appears to be the most appropriate time zero compared to other cases.

4. Conclusion

This study attempted to use superabsorbent polymer (SAP) as a rheology modifier for modifying the rheology and structural build-up of fresh cementitious materials. The effect of SAP on flow behaviors, structural build-up, hydration kinetics, compressive strength, and autogenous shrinkage of limestone-calcined clay-based cement (LC3) pastes with a relatively low W/B (0.3) has been studied. The main findings based on test results can be summarized as follows.

- In the flow regime, increasing SAP dosage increased the dynamic yield stress and the apparent viscosity of LC3 pastes due to the water uptake of SAP. The addition of VMA further boosted both values, relying on water absorption and bridging flocculation. Dynamic yield stress and apparent viscosity were reduced by increasing SP dosage, which may be related to the reduction in water absorption of SAP. The flow curve of mixtures without VMA displayed shear-thickening behavior (10–100 s^{-1}), whereas a shear-thinning property (10–100 s^{-1}) was observed after adding 0.1 wt% VMA.
- The critical strain of fresh LC3 pastes was decreased by adding SAP and/or VMA in the amplitude sweep test (started at 8 min). Furthermore, using SAP (only SAP or SAP + VMA) appeared to reduce the free water content and the mean interparticle distance in the fresh mixture, promoting the structural build-up of LC3 pastes during 22–72 min. Conversely, the structuration of LC3 pastes was delayed by only adding 0.1 wt% VMA or increasing SP dosage from 0.8 wt% to 1 wt%.
- During the first 24 h, hydration of LC3 was accelerated and enhanced by adding only 0.1 wt% SAP (mixture A1) or 0.1 wt% VMA (mixture B1), whereas C_3S hydration was attenuated by further addition of 0.1 wt% SAP (mixture A2) or 0.2 wt% SP (mixture A3). Compared to the REF mixture, mixtures with SAP and/or VMA showed a higher cumulative heat and portlandite content at 7 days, probably due to their internal curing effects. Also, the compressive strength of LC3 paste at 3, 7, and 28 days was decreased by adding SAP (with or without increased SP) and/or VMA. Both SAP and VMA increased the air void content of the cementitious matrix, thereby negatively affecting the compressive strength.
- When the time-zero was defined as 12 h, the use of SAP (especially adding 0.2 wt% SAP) not only contributed to the growth of expansion peak on the first day but also effectively mitigated the autogenous shrinkage of LC3 pastes over 7 days. The addition of 0.1 wt% VMA (mixtures B1 and B2) appeared to alleviate autogenous shrinkage compared to the REF.
- The obtained results indicated that SAP could act as a promising rheology modifier for the development of 3D printable cementitious materials. Compared to HPMC-based VMA, the addition of SAP results in less flowability sacrifice, considerable improvement of structural build-up and autogenous shrinkage. Please note that all conclusions in this work are based on a specific SAP. The influences on rheology, hydration kinetics, strength and internal curing may vary if a different type of SAP is used.

CRediT authorship contribution statement

Yu Chen: Conceptualization, Methodology, Formal analysis, Investigation, Data curation, Writing – original draft, Writing – review & editing. **Minfei Liang:** Conceptualization, Methodology, Formal analysis, Investigation, Data curation, Writing – original draft, Writing – review & editing. **Yu Zhang:** Investigation, Writing – review & editing. **Zhenming Li:** Investigation, Writing – review & editing. **Branko Šavija:** Supervision, Funding acquisition, Writing – review & editing. **Erik Schlangen:** Supervision, Funding acquisition, Writing – review & editing. **Oğuzhan Çopuroğlu:** Supervision, Funding acquisition, Writing – review & editing.

Declaration of Competing Interest

The authors declare that they have no known competing financial interests or personal relationships that could have appeared to influence the work reported in this paper.

Data availability

Data will be made available on request.

Acknowledgments

Minfei Liang and Yu Zhang would like to acknowledge the funding supported by China Scholarship Council under grant No. 202007000027, 201808320456. Dr. Branko Šavija acknowledges the financial support of the European Research Council (ERC) within the framework of the ERC Starting Grant Project “Auxetic Cementitious Composites by 3D printing (ACC-3D)”, Grant Agreement Number 101041342.

References

[1] M.C.G. Juenger, F. Winnefeld, J.L. Provis, J.H. Ideker, Advances in alternative cementitious binders, Cem. Concr. Res. 41 (2011) 1232–1243, https://doi.org/10.1016/j.cemconres.2010.11.012.
[2] K. Scrivener, F. Martirena, S. Bishnoi, S. Maity, Calcined clay limestone cements (LC3), Cem. Concr. Res. 114 (2018) 49–56, https://doi.org/10.1016/j.cemconres.2017.08.017.
[3] R. Snellings, Assessing, Understanding and Unlocking Supplementary Cementitious Materials, RILEM Tech. Lett. 1 (2016) 50. doi:10.21809/rilemtechlett.2016.12.
[4] F. Zunino, K. Scrivener, Microstructural developments of limestone calcined clay cement (LC3) pastes after long-term (3 years) hydration, Cem. Concr. Res. 153 (2022), 106693, https://doi.org/10.1016/j.cemconres.2021.106693.
[5] M. Sharma, S. Bishnoi, F. Martirena, K. Scrivener, Limestone calcined clay cement and concrete: A state-of-the-art review, Cem. Concr. Res. 149 (2021), 106564, https://doi.org/10.1016/j.cemconres.2021.106564.
[6] F. Zunino, K. Scrivener, The influence of the filler effect on the sulfate requirement of blended cements, Cem. Concr. Res. 126 (2019), 105918, https://doi.org/10.1016/j.cemconres.2019.105918.
[7] F. Avet, K. Scrivener, Investigation of the calcined kaolinite content on the hydration of Limestone Calcined Clay Cement (LC3), Cem. Concr. Res. 107 (2018) 124–135, https://doi.org/10.1016/j.cemconres.2018.02.016.
[8] Z. Shi, M.R. Geiker, K. De Weerdt, T.A. Østnor, B. Lothenbach, F. Winnefeld, J. Skibsted, Role of calcium on chloride binding in hydrated Portland cement–metakaolin–limestone blends, Cem. Concr. Res. 95 (2017) 205–216, https://doi.org/10.1016/j.cemconres.2017.02.003.
[9] Y. Dhandapani, M. Santhanam, Investigation on the microstructure-related characteristics to elucidate performance of composite cement with limestone-calcined clay combination, Cem. Concr. Res. 129 (2020), 105959, https://doi.org/10.1016/j.cemconres.2019.105959.
[10] Q.D. Nguyen, T. Kim, A. Castel, Mitigation of alkali-silica reaction by limestone calcined clay cement (LC3), Cem. Concr. Res. 137 (2020), 106176, https://doi.org/10.1016/j.cemconres.2020.106176.
[11] K. Scrivener, F. Avet, H. Maraghechi, F. Zunino, J. Ston, W. Hanpongpun, A. Favier, Impacting factors and properties of limestone calcined clay cements (LC 3), Green Mater. 7 (2018) 3–14, https://doi.org/10.1680/jgrma.18.00029.
[12] Q.D. Nguyen, S. Afroz, Y. Zhang, T. Kim, W. Li, A. Castel, Autogenous and total shrinkage of limestone calcined clay cement (LC3) concretes, Constr. Build. Mater. 314 (2022), 125720, https://doi.org/10.1016/j.conbuildmat.2021.125720.
[13] V. Baroghel-Bouny, P. Mounanga, A. Khelidj, A. Loukili, N. Rafaï, Autogenous deformations of cement pastes: Part II. W/C effects, micro-macro correlations, and threshold values, Cem. Concr. Res. 36 (2006) 123–136, https://doi.org/10.1016/j.cemconres.2004.10.020.
[14] R. Hay, L. Li, K. Celik, Shrinkage, hydration, and strength development of limestone calcined clay cement (LC3) with different sulfation levels, Cem. Concr. Compos. 127 (2022), 104403, https://doi.org/10.1016/j.cemconcomp.2021.104403.
[15] T. Lu, Z. Li, K. van Breugel, Modelling of autogenous shrinkage of hardening cement paste, Constr. Build. Mater. 264 (2020), 120708, https://doi.org/10.1016/j.conbuildmat.2020.120708.
[16] H. Du, S.D. Pang, High-performance concrete incorporating calcined kaolin clay and limestone as cement substitute, Constr. Build. Mater. 264 (2020), 120152, https://doi.org/10.1016/j.conbuildmat.2020.120152.
[17] Y. Chen, S. He, Y. Zhang, Z. Wan, O. Çopuroğlu, E. Schlangen, 3D printing of calcined clay-limestone-based cementitious materials, Cem. Concr. Res. 149 (2021), 106553, https://doi.org/10.1016/j.cemconres.2021.106553.
[18] Y. Chen, C.R. Rodriguez, Z. Li, B. Chen, O. Çopuroğlu, E. Schlangen, Effect of different grade levels of calcined clays on fresh and hardened properties of ternary-

blended cementitious materials for 3D printing, Cem. Concr. Compos. 114 (2020), 103708, https://doi.org/10.1016/j.cemconcomp.2020.103708.
[19] Y. Chen, S. Chaves Figueiredo, Z. Li, Z. Chang, K. Jansen, O. Çopuroğlu, E. Schlangen, Improving printability of limestone-calcined clay-based cementitious materials by using viscosity-modifying admixture, Cem. Concr. Res. 132 (2020), 106040, https://doi.org/10.1016/j.cemconres.2020.106040.
[20] O.M. Jensen, P.F. Hansen, Autogenous deformation and RH-change in perspective, Cem. Concr. Res. 31 (2001) 1859–1865, https://doi.org/10.1016/S0008-8846(01)00501-4.
[21] O.M. Jensen, P. Lura, Techniques and materials for internal water curing of concrete, Mater. Struct. Constr. 39 (2006) 817–825, https://doi.org/10.1617/s11527-006-9136-6.
[22] X. Yuanliang, Z. Chao, C. Chun, Z. Yamei, Effect of superabsorbent polymer on the foam-stability of foamed concrete, Cem. Concr. Compos. 127 (2022), 104398, https://doi.org/10.1016/j.cemconcomp.2021.104398.
[23] Z. He, A. Shen, Y. Guo, Z. Lyu, D. Li, X. Qin, M. Zhao, Z. Wang, Cement-based materials modified with superabsorbent polymers: A review, Constr. Build. Mater. 225 (2019) 569–590, https://doi.org/10.1016/j.conbuildmat.2019.07.139.
[24] D. Snoeck, D. Schaubroeck, P. Dubruel, N. De Belie, Effect of high amounts of superabsorbent polymers and additional water on the workability, microstructure and strength of mortars with a water-to-cement ratio of 0.50, Constr. Build. Mater. 72 (2014) 148–157, https://doi.org/10.1016/j.conbuildmat.2014.09.012.
[25] B. Sun, H. Wu, W. Song, Z. Li, J. Yu, Design methodology and mechanical properties of Superabsorbent Polymer (SAP) cement-based materials, Constr. Build. Mater. 204 (2019) 440–449, https://doi.org/10.1016/j.conbuildmat.2019.01.206.
[26] S.H. Kang, S.G. Hong, J. Moon, Absorption kinetics of superabsorbent polymers (SAP) in various cement-based solutions, Cem. Concr. Res. 97 (2017) 73–83, https://doi.org/10.1016/j.cemconres.2017.03.009.
[27] J. Liu, N. Farzadnia, C. Shi, X. Ma, Effects of superabsorbent polymer on shrinkage properties of ultra-high strength concrete under drying condition, Constr. Build. Mater. 215 (2019) 799–811, https://doi.org/10.1016/j.conbuildmat.2019.04.237.
[28] V. Mechtcherine, M. Gorges, C. Schroefl, A. Assmann, W. Brameshuber, A. B. Ribeiro, D. Cusson, J. Custódio, E.F. Da Silva, K. Ichimiya, S.I. Igarashi, A. Klemm, K. Kovler, A.N. De Mendonça Lopes, P. Lura, V.T. Nguyen, H. W. Reinhardt, R.D.T. Filho, J. Weiss, M. Wyrzykowski, G. Ye, S. Zhutovsky, Effect of internal curing by using superabsorbent polymers (SAP) on autogenous shrinkage and other properties of a high-performance fine-grained concrete: Results of a RILEM round-robin test, Mater. Struct. Constr. 47 (2014) 541–562, https://doi.org/10.1617/s11527-013-0078-5.
[29] V. Mechtcherine, C. Schröfl, M. Wyrzykowski, M. Gorges, P. Lura, D. Cusson, J. Margeson, N. De Belie, D. Snoeck, K. Ichimiya, S.I. Igarashi, V. Falikman, S. Friedrich, J. Bokern, P. Kara, A. Marciniak, H.W. Reinhardt, S. Sippel, A. Bettencourt Ribeiro, J. Custódio, G. Ye, H. Dong, J. Weiss, Effect of superabsorbent polymers (SAP) on the freeze–thaw resistance of concrete: results of a RILEM interlaboratory study, Mater. Struct. Constr. 50 (2017), https://doi.org/10.1617/s11527-016-0868-7.
[30] V. Mechtcherine, E. Secrieru, C. Schröfl, Effect of superabsorbent polymers (SAPs) on rheological properties of fresh cement-based mortars - Development of yield stress and plastic viscosity over time, Cem. Concr. Res. 67 (2015) 52–65, https://doi.org/10.1016/j.cemconres.2014.07.003.
[31] E. Secrieru, V. Mechtcherine, C. Schröfl, D. Borin, Rheological characterisation and prediction of pumpability of strain-hardening cement-based-composites (SHCC) with and without addition of superabsorbent polymers (SAP) at various temperatures, Constr. Build. Mater. 112 (2016) 581–594, https://doi.org/10.1016/j.conbuildmat.2016.02.161.
[32] X. Ma, Q. Yuan, J. Liu, C. Shi, Effect of water absorption of SAP on the rheological properties of cement-based materials with ultra-low w/b ratio, Constr. Build. Mater. 195 (2019) 66–74, https://doi.org/10.1016/j.conbuildmat.2018.11.050.
[33] H. Paiva, A. Velosa, P. Cachim, V.M. Ferreira, Effect of metakaolin dispersion on the fresh and hardened state properties of concrete, Cem. Concr. Res. 42 (2012) 607–612, https://doi.org/10.1016/j.cemconres.2012.01.005.
[34] N. Nair, K. Mohammed Haneefa, M. Santhanam, R. Gettu, A study on fresh properties of limestone calcined clay blended cementitious systems, Constr. Build. Mater. 254 (2020) 119326. doi:10.1016/j.conbuildmat.2020.119326.
[35] Y. Chen, S. He, Y. Gan, O. Çopuroğlu, F. Veer, E. Schlangen, A review of printing strategies, sustainable cementitious materials and characterization methods in the context of extrusion-based 3D concrete printing, J. Build. Eng. 45 (2022), 103599, https://doi.org/10.1016/j.jobe.2021.103599.
[36] A.V. Rahul, M. Santhanam, H. Meena, Z. Ghani, 3D printable concrete: Mixture design and test methods, Cem. Concr. Compos. 97 (2019) 13–23, https://doi.org/10.1016/j.cemconcomp.2018.12.014.
[37] M. Chen, L. Li, Y. Zheng, P. Zhao, L. Lu, X. Cheng, Rheological and mechanical properties of admixtures modified 3D printing sulphoaluminate cementitious materials, Constr. Build. Mater. 189 (2018) 601–611, https://doi.org/10.1016/j.conbuildmat.2018.09.037.
[38] M.T. Hasholt, O.M. Jensen, K. Kovler, S. Zhutovsky, Can superabsorent polymers mitigate autogenous shrinkage of internally cured concrete without compromising the strength? Constr. Build. Mater. 31 (2012) 226–230, https://doi.org/10.1016/j.conbuildmat.2011.12.062.
[39] J. Justs, M. Wyrzykowski, F. Winnefeld, D. Bajare, P. Lura, Influence of superabsorbent polymers on hydration of cement pastes with low water-to-binder ratio: A calorimetry study, J. Therm. Anal. Calorim. 115 (2014) 425–432, https://doi.org/10.1007/s10973-013-3359-x.
[40] J. Justs, M. Wyrzykowski, D. Bajare, P. Lura, Internal curing by superabsorbent polymers in ultra-high performance concrete, Cem. Concr. Res. 76 (2015) 82–90, https://doi.org/10.1016/j.cemconres.2015.05.005.
[41] C.R. Rodriguez, M. Deprez, F.F. de Mendonca Filho, S. van Offenwert, V. Cnudde, E. Schlangen, B. Šavija, X-Ray Micro Tomography of Water Absorption by Superabsorbent Polymers in Mortar, in: W. Boshoff, R. Combrinck, V. Mechtcherine, M. Wyrzykowski (Eds.), 3rd Int. Conf. Appl. Superabsorbent Polym. Other New Admixtures Towar. Smart Concr. SAP 2019, Springer International Publishing, 2020, pp. 29–37. doi:10.1007/978-3-030-33342-3_4.
[42] V. Mechtcherine, D. Snoeck, C. Schröfl, N. De Belie, A.J. Klemm, K. Ichimiya, J. Moon, M. Wyrzykowski, P. Lura, N. Toropovs, A. Assmann, S. Igarashi, I. De La Varga, F.C.R. Almeida, K. Erk, A.B. Ribeiro, J. Custódio, H.W. Reinhardt, V. Falikman, Testing superabsorbent polymer (SAP) sorption properties prior to implementation in concrete: results of a RILEM Round-Robin Test, Mater. Struct. Constr. 51 (2018), https://doi.org/10.1617/s11527-018-1149-4.
[43] D. Snoeck, C. Schröfl, V. Mechtcherine, Recommendation of RILEM TC 260-RSC: testing sorption by superabsorbent polymers (SAP) prior to implementation in cement-based materials, Mater. Struct. Constr. 51 (2018), https://doi.org/10.1617/s11527-018-1242-8.
[44] S. Zhao, O.M. Jensen, M.T. Hasholt, X. Guan, Absorption capacity of superabsorbent polymer in cement pastes: a robustness test, Mater. Struct. Constr. 54 (2021) 1–15, https://doi.org/10.1617/s11527-021-01636-7.
[45] Y. Chen, Y. Zhang, S. He, X. Liang, E. Schlangen, O. Çopuroğlu, Improving structural build-up of limestone-calcined clay-cement pastes by using inorganic additives, Under Rev. (n.d.).
[46] X. Dai, S. Aydın, M.Y. Yardımcı, K. Lesage, G. De Schutter, Effects of activator properties and GGBFS/FA ratio on the structural build-up and rheology of AAC, Cem. Concr. Res. 138 (2020), 106253, https://doi.org/10.1016/j.cemconres.2020.106253.
[47] Q. Yuan, D. Zhou, K.H. Khayat, D. Feys, C. Shi, On the measurement of evolution of structural build-up of cement paste with time by static yield stress test vs. small amplitude oscillatory shear test, Cem. Concr. Res. 99 (2017) 183–189, https://doi.org/10.1016/j.cemconres.2017.05.014.
[48] D. Jiao, K. El Cheikh, C. Shi, K. Lesage, G. De Schutter, Structural build-up of cementitious paste with nano-Fe3O4 under time-varying magnetic fields, Cem. Concr. Res. (2019), https://doi.org/10.1016/j.cemconres.2019.105857.
[49] S. Ma, Y. Qian, S. Kawashima, Experimental and modeling study on the non-linear structural build-up of fresh cement pastes incorporating viscosity modifying admixtures, Cem. Concr. Res. 108 (2018) 1–9, https://doi.org/10.1016/j.cemconres.2018.02.022.
[50] X. Dai, S. Aydin, M. Yücel Yardimci, R.E.N. Qiang, K. Lesage, G. De Schutter, Rheology, early-age hydration and microstructure of alkali-activated GGBFS-Fly ash-limestone mixtures, Cem. Concr. Compos. 124 (2021), 104244, https://doi.org/10.1016/j.cemconcomp.2021.104244.
[51] M.A. Schultz, L.J. Struble, Use of oscillatory shear to study flow behavior of fresh cement paste, Cem. Concr. Res. 23 (1993) 273–282, https://doi.org/10.1016/0008-8846(93)90092-N.
[52] Q. Yuan, X. Lu, K.H. Khayat, D. Feys, C. Shi, Small amplitude oscillatory shear technique to evaluate structural build-up of cement paste, Mater. Struct. Constr. 50 (2017) 1–12, https://doi.org/10.1617/s11527-016-0978-2.
[53] X. Dai, Q. Ren, S. Aydın, M.Y. Yardımcı, K. Lesage, G. De Schutter, Enhancing thixotropy and structural build-up of alkali-activated slag/fly ash pastes with nano clay, Mater. Struct. Constr. 54 (2021), https://doi.org/10.1617/s11527-021-01760-4.
[54] T.G. Mezger, The Rheology Handbook, 4th ed., Emerald Group Publishing Limited, 2009. doi:10.1108/prt.2009.12938eac.006.
[55] B. Lothenbach, P. Durdzinski, K. De Weerdt, Thermogravimetric analysis, in: K. Scrivener, R. Snellings, B. Lothenbach (Eds.), A Pract. Guid. to Microstruct. Anal. Cem. Mater., CRC Press, 2016, pp. 177–212.
[56] NEN-EN 196-1, Methods of testing cement – Part 1: Determination of strength, (2016).
[57] Y. Chen, O. Çopuroğlu, C.R. Rodriguez, F.F. de Mendonca Filho, E. Schlangen, Characterization of air-void systems in 3D printed cementitious materials using optical image scanning and X-ray computed tomography, Mater. Charact. 173 (2021), 110948, https://doi.org/10.1016/j.matchar.2021.110948.
[58] NEN-EN 196-3, Methods of testing cement. Determination of setting times and soundness, NEN. (2016) 18. https://shop.bsigroup.com.
[59] ASTM C1698-19, Standard Test Method for Autogenous Strain of Cement Paste and Mortar, ASTM Int. 04 (2019) 1–8. doi:10.1520/C1698-19.2.
[60] M. Palacios, R.J. Flatt, Working mechanism of viscosity-modifying admixtures, Elsevier Ltd (2015), https://doi.org/10.1016/B978-0-08-100693-1.00020-5.
[61] K.H. Khayat, N. Mikanovic, Viscosity-enhancing admixtures and the rheology of concrete, Woodhead Publishing Limited (2011), https://doi.org/10.1016/B978-0-85709-028-7.50008-X.
[62] H. Bessaies-Bey, M. Palacios, E. Pustovgar, M. Hanafi, R. Baumann, R.J. Flatt, N. Roussel, Non-adsorbing polymers and yield stress of cement paste: Effect of depletion forces, Cem. Concr. Res. 111 (2018) 209–217, https://doi.org/10.1016/j.cemconres.2018.05.004.
[63] N. Roussel, A. Lemaître, R.J. Flatt, P. Coussot, Steady state flow of cement suspensions: A micromechanical state of the art, Cem. Concr. Res. 40 (2010) 77–84, https://doi.org/10.1016/j.cemconres.2009.08.026.
[64] Y. Chen, Y. Zhang, S. He, M. Liang, Y. Zhang, E. Schlangen, O. Çopuroğlu, Effect of different metakaolin contents on rheology and structural build-up of limestone-calcined clay-cement pastes, Submitted. (n.d.).
[65] N. Roussel, G. Ovarlez, S. Garrault, C. Brumaud, The origins of thixotropy of fresh cement pastes, Cem. Concr. Res. 42 (2012) 148–157, https://doi.org/10.1016/j.cemconres.2011.09.004.
[66] J. Mewis, N.J. Wagner, Thixotropy, Adv. Colloid Interface Sci. 147–148 (2009) 214–227, https://doi.org/10.1016/j.cis.2008.09.005.

[67] N. Roussel, H. Bessaies-Bey, S. Kawashima, D. Marchon, K. Vasilic, R. Wolfs, Recent advances on yield stress and elasticity of fresh cement-based materials, Cem. Concr. Res. 124 (2019), 105798, https://doi.org/10.1016/j.cemconres.2019.105798.
[68] G. Gelardi, R.J. Flatt, Working mechanisms of water reducers and superplasticizers, Elsevier Ltd (2015), https://doi.org/10.1016/B978-0-08-100693-1.00011-4.
[69] D. Marchon, S. Kawashima, H. Bessaies-Bey, S. Mantellato, S. Ng, Hydration and rheology control of concrete for digital fabrication: Potential admixtures and cement chemistry, Cem. Concr. Res. 112 (2018) 96–110, https://doi.org/10.1016/j.cemconres.2018.05.014.
[70] D. Marchon, R.J. Flatt, Impact of chemical admixtures on cement hydration, Elsevier Ltd (2015), https://doi.org/10.1016/B978-0-08-100693-1.00012-6.
[71] S. Gauffinet-Garrault, The rheology of cement during setting, in: Underst. Rheol. Concr., Elsevier, 2012: pp. 96–113. 10.1533/9780857095282.1.96.
[72] E. Berodier, K. Scrivener, G. Scherer, Understanding the Filler Effect on the Nucleation and Growth of C-S-H, J. Am. Ceram. Soc. 97 (12) (2014) 3764–3773.
[73] C. Brumaud, R. Baumann, M. Schmitz, M. Radler, N. Roussel, Cellulose ethers and yield stress of cement pastes, Cem. Concr. Res. 55 (2014) 14–21, https://doi.org/10.1016/j.cemconres.2013.06.013.
[74] P. Steins, A. Poulesquen, O. Diat, F. Frizon, Structural evolution during geopolymerization from an early age to consolidated material, Langmuir. 28 (2012) 8502–8510, https://doi.org/10.1021/la300868v.
[75] S. Chaves Figueiredo, O. Çopuroğlu, E. Schlangen, Effect of viscosity modifier admixture on Portland cement paste hydration and microstructure, Constr. Build. Mater. 212 (2019) 818–840, https://doi.org/10.1016/j.conbuildmat.2019.04.020.
[76] K. De Weerdt, M. Ben Haha, G. Le Saout, K.O. Kjellsen, H. Justnes, B. Lothenbach, Hydration mechanisms of ternary Portland cements containing limestone powder and fly ash, Cem. Concr. Res. 41 (2011) 279–291, https://doi.org/10.1016/j.cemconres.2010.11.014.
[77] F. Zunino, K. Scrivener, The reaction between metakaolin and limestone and its effect in porosity refinement and mechanical properties, Cem. Concr. Res. 140 (2021), 106307, https://doi.org/10.1016/j.cemconres.2020.106307.
[78] M. Liang, Z. Li, S. He, Z. Chang, Y. Gan, E. Schlangen, B. Šavija, Stress evolution in restrained GGBFS concrete due to autogenous deformation: bayesian optimization of aging creep, Constr. Build. Mater. 324 (2022), https://doi.org/10.1016/j.conbuildmat.2022.126690.
[79] M. Liang, Z. Chang, Z. Wan, Y. Gan, E. Schlangen, B. Šavija, Interpretable Ensemble-Machine-Learning models for predicting creep behavior of concrete, Cem. Concr. Compos. 125 (2022), https://doi.org/10.1016/j.cemconcomp.2021.104295.
[80] L. Minfei, G. Yidong, C. Ze, W. Zhi, S. Erik, Š. Branko, Microstructure-informed deep convolutional neural network for predicting short-term creep modulus of cement paste, Cem. Concr. Res. 152 (2022), https://doi.org/10.1016/j.cemconres.2021.106681.
[81] A. Darquennes, S. Staquet, M.P. Delplancke-Ogletree, B. Espion, Effect of autogenous deformation on the cracking risk of slag cement concretes, Cem. Concr. Compos. 33 (2011) 368–379, https://doi.org/10.1016/j.cemconcomp.2010.12.003.
[82] A. Darquennes, S. Staquet, B. Espion, Determination of time-zero and its effect on autogenous deformation evolution, Eur. J. Environ. Civ. Eng. 15 (2011) 1017–1029, https://doi.org/10.1080/19648189.2011.9695290.
[83] J.R.T. Filho, M.A.P.G. de Araújo, D. Snoeck, N. De Belie, Discussing different approaches for the time-zero as start for autogenous shrinkage in cement pastes containing superabsorbent polymers, Materials (Basel) 12 (2019), https://doi.org/10.3390/ma12182962.
[84] Y. Ma, X. Yang, J. Hu, Z. Zhang, H. Wang, Accurate determination of the "time-zero" of autogenous shrinkage in alkali-activated fly ash/slag system, Compos. Part B Eng. 177 (2019), https://doi.org/10.1016/j.compositesb.2019.107367.